MV^{2}Net: Multi-Variate Multi-View Brain Network Comparison over Uncertain Data

Lei Shi, Junnan Hu, Zhihao Tan, Jun Tao, Jiayan Ding, Yan Jin, Yanjun Wu, and Paul M. Thompson

Abstract—Visually identifying effective bio-markers from human brain networks poses non-trivial challenges to the field of data visualization and analysis. Existing methods in the literature and neuroscience practice are generally limited to the study of individual connectivity features in the brain (e.g., the strength of neural connection among brain regions). Pairwise comparisons between contrasting subject groups (e.g., the diseased and the healthy controls) are normally performed. The underlying neuroimaging and brain network construction process is assumed to have 100% fidelity. Yet, real-world user requirements on brain network visual comparison lean against these assumptions. In this work, we present MV^{2}Net, a visual analytics system that tightly integrates multi-variate multi-view visualization for brain network comparison with an interactive wrangling mechanism to deal with data uncertainty. On the analysis side, the system integrates multiple extraction methods on diffusion and geometric connectivity features of brain networks, an anomaly detection algorithm for data quality assessment, single- and multi-connection feature selection methods for bio-marker detection. On the visualization side, novel designs are introduced which optimize network comparisons among contrasting subject groups and related connectivity features. Our design provides level-of-detail comparisons, from juxtaposed and explicit-coding views for subject group comparisons, to high-order composite view for correlation of network comparisons, and to fiber tract detail view for voxel-level comparisons. The proposed techniques are inspired and evaluated in expert studies, as well as through case analyses on diffusion and geometric bio-markers of certain neurology diseases. Results in these experiments demonstrate the effectiveness and superiority of MV^{2}Net over state-of-the-art approaches.

Index Terms—Brain network, visual comparison, multivariate analysis

1 Introduction

Visually analyzing human brain networks for bio-marker detection is a known problem in visualization research. Here the bio-marker refers to the indicator in brain networks for certain neurology diseases. This work focuses on the structural brain network estimated from multimodal magnetic resonance imaging (MRI) data (T1, T2, diffusion, etc.) where network nodes are defined by brain regions in the cortical level and edges are defined by neural fibers connecting the regions. The brain networks of the diseased subject group and the control group are compared to extract discriminative network connections. The discriminative connections are certain connectivity features significantly different between the brain networks of the two groups in the statistical test, which could be potential bio-markers of the disease under study. Recent literature in neuroscience and computer science have validated many network bio-markers in the human brain that are associated with neurology diseases (e.g., the alzheimer's disease (AD) [1], schizophrenia [2]) or genetic disorders [3]. These findings can be critical for disease prevention and treatment.

Visualization has been an effective technique in comparing complex networks [4] (e.g., routing diagrams, dynamic social networks). The interactive interface promotes users in spotting differences and understanding the output of comparison algorithms. Nevertheless, on comparing brain networks for bio-marker detection, existing visualization approaches are far from optimal. Domain users, including doctors and neuroscience researchers, are not using visualization as a primary method in their clinical practice. First, users are generally satisfied with 3D visualizations of reconstructed fiber connectivity on a single brain [5] [6]. Yet, aligning fibers of hundreds of subjects in the same 3D space is extremely difficult, if not impossible at all. Most solutions simplify brain connectivity into single-weight edges among cortical regions where the edge weight indicates the number of brain fibers on each connection (i.e., the strength). These weighted brain networks can be effectively aggregated and compared in groups, but at the cost of missing bio-markers on the other connectivity features. For example, diffusion features such as fractional anisotropy (FA) are known to be indicators of the brain network integrity. Brain tumors can not be identified because of the unaffected number of fibers. Second, state-of-the-art brain network comparisons mostly adopt a single-view approach that juxtaposes or superimposes two groups of networks at a time. The actual task of domain users could involve more than one group-based comparison, e.g., alzheimer's disease (AD) v.s. control and frontotemporal dementia (FTD) v.s. control for AD-specific bio-markers. This is not explicitly supported in previous visualization designs. Third, domain users are concerned with the uncertainty of neuroimaging and brain network construction. They could make wrong decisions due to the

- *Lei Shi is with SKLSDE and Beijing Advanced Innovation Center for Big Data and Brain Computing, School of Computer Science and Engineering, Beihang University, China. Email: leishi@buaa.edu.cn.*
- *Junnan Hu and Jun Tao are with School of Data and Computer Science in Sun Yat-sen University and National Supercomputer Center at Guangzhou, China. Email: hujn3@mail2.sysu.edu.cn, taoj23@mail.sysu.edu.cn.*
- *Zhihao Tan and Yanjun Wu are with Institute of Software, Chinese Academy of Sciences, China. Email: tanzhihao18@mails.ucas.edu.cn, yanjun@iscas.ac.cn.*
- *Jiayan Ding is with College of Design and Innovation, Tongji University, China. Email: dingjy@tongji.edu.cn.*
- *Yan Jin is with Department of Radiation Oncology, The University of Texas MD Anderson Cancer Center, USA. E-mail: yjinz@ucla.edu.*
- *Paul M. Thompson is with the Imaging Genetics Center, Mark and Mary Stevens Institute for Neuroimaging and Informatics, University of Southern California, USA. E-mail: pthomp@usc.edu.*

data quality issue. But most of the current systems do not support the analysis of data quality in the visual analytics process.

In this work, we collected user requirements on brain network comparison in a pilot user study with domain experts. To meet the user requirement, a visual analytics system called MV^{2}Net is introduced, which proposes Multi-Variate Multi-View brain NETwork comparison over uncertain data. On the data uncertainty issue, an interactive data wrangling mechanism is designed to identify low-quality connectivity features, filter them out, and still carry out a comparison on reliable components of brain networks. To achieve a comprehensive brain network comparison, we extract both the strength of a network connection and its diffusion and geometric features (FA, curvature, etc.). These features are selected via discriminative feature selection algorithms and displayed through multi-variate visualizations simultaneously. To fulfill high-order comparison tasks on brain networks, a multi-view design is proposed with customized user interaction support.

We make the following contributions in MV^{2}Net:

- An end-to-end **analysis framework** to extract, assess, manage, and compare diffusion and geometric connectivity features on the human brain network. Notably, an anomaly detection algorithm is applied to extract low-quality connectivity features based on their characteristics and distributions. Both statistical tests for univariate discriminative feature selection and group-based multivariate feature selection algorithms are introduced to detect single and block bio-markers from multiple connectivity features in contrasting subject group's brain networks. (Section 4)
- The level-of-detail **visualization design** for multi-variate multi-group comparison over brain networks. Coordinated multiple views are presented which include side-by-side and explicit-coding visual network comparison on individual features, a composite brain necklace visualization for correlation and comparison of multiple features simultaneously, and juxtaposed 3D visualizations of fiber tracts which reveal detailed affected regions of the diseased subjects. (Section 5)
- The system **implementation and evaluation** of MV^{2}Net through two application case studies and the expert feedback. The experiments validate the effectiveness and superiority of MV^{2}Net over univariate, single-view visual comparison approaches. Note that our result on geometric connectivity features and the correlation among multivariate diffusion features have not been shown by existing visualization tools. The system also supports the incorporation of new brain connectivity features in the visual comparison analysis process. (Section 6)

2 Related Work

2.1 Brain Network Visualization

Visualization is an effective tool to understand human brain networks estimated from neuroimaging data. By far the most widespread visual representations are node-link graphs and adjacency matrices, e.g., in software tools [7], textbooks [8], and review papers [9]. On node-link graphs, researches have been conducted to accommodate traditional network layouts in the brain network scenario. Worsley et al. depicted human brain networks in a 3D space using projections on three anatomical planes [10]. Salvador et al. applied dimensionality reduction algorithms such as MDS to reveal the functional similarity among nodes defined by region of interest (ROI) [11]. Mcgonigle et al. introduced the ChordMap metaphor to display the hierarchical connectivity of brain networks [12]. On the other hand, matrix representations [13] are also favored because brain graphs often have medium to large sizes and are considerably dense [14]. Notably, Alper et al. studied the use of node-link and matrix representations in weighted brain graph comparison [15]. Their result recommended a specific overlaid matrix design. To enjoy the best world of both node-link graph and matrix, Yang et al. applied the NodeTrix metaphor in visually detecting blockwise patterns between contrasting groups of brain networks [16].

Visualizations were also studied on specific types of brain networks. Pandey et al. proposed CerebroVis, an abstract visualization design for cerebral artery networks, which uses a constrained layout algorithm to preserve spatial context [17]. Bach et al. visually explored the temporal dynamics of functional brain networks and invented novel designs to discover useful patterns from dynamic brain networks. Matrix Cubes combined the classical adjacency matrix design with a third time dimension to create the 3D cube visual metaphor [18]. Small Multipiles aggregates a time series of dynamic brain networks into multiple clusters according to matrix similarity [19]. A pile-based design is introduced to visually represent each cluster, with a cover matrix selected from each pile to summarize the brain network of that pile. Time Curves maps a series of dynamic networks into a curve connecting multiple points [20]. NeuroLines [21] and Abstractocyte [22] are proposed to visualize microscopic brain networks such as neural connectivity, which is not the focus of this work. For literature review on brain network visualization, we refer to systematic surveys [23] [24].

In the literature, researchers have studied visualization of multivariate networks that have rich semantics on network nodes (e.g., role types in academic networks, user demographics in social networks). Wattenberg invented PivotGraph [25], a node-link representation of networks aggregated by a flexible combination of node attributes. Shneiderman and Aris developed Semantic Substrate [26], a user-defined visualization method for multivariate networks that layouts nodes into non-overlapping regions by their attributes. Nobre et al. proposed Juniper [27], a tree+table visualization technique that illustrates both topology and rich node attributes of multivariate networks by querying and focusing on user-selected nodes and subgraphs. These existing approaches can be applied to brain networks measured at multiple scales and modalities, which have rich attributes on brain network nodes. Yet, on our structural brain networks derived from DTI data, nodes (i.e., region of interests (ROI)) generally have few attributes useful for visualization. Exceptions are anatomical parcellation and clustering information of ROIs, which can be used to visually abstract brain networks [16] [12]. In neuroscience, the most studied network attribute might be subject demographics, e.g., networks can be aggregated by diagnostic groups for bio-marker detection.

Compared with existing brain network visualizations, our work is motivated by a less investigated problem of visualizing and comparing multiple connectivity features (i.e., edge attributes) on brain networks. Recent studies on neuroscience have called for the analysis of diffusion and geometric connectivity features beyond the classical fiber count/strength measure on brain networks [28] [29]. According to the latest survey on multivariate network visualization [30], most approaches modify common visual encoding channels, e.g., line width, color, or pattern, to represent one edge attribute [31] [32]. Few methods are designed to reveal the pattern of multiple edge attributes simultaneously. One exception is the design by Schöffel et al. which applied colored bar charts to display many

edge attributes [33]. In Section 5.1, we have discussed our design rationale in comparison to Schöffel et al.'s work.

We note that beyond the visualization of brain white matter connectivity, Jönsson et al. recently proposed VisualNeuro [34], a neuroimaging application that visually analyzes functional MRI (fMRI) data in the voxel level. Similar to our approach, VisualNeuro supports the comparison between user-defined subject groups and combines statistical analysis with interactive visualization to illustrate significant differences between the subject groups. Comparing our MV^{2}Net system with VisualNeuro, we work with multiple brain connectivity features and support the display of multiple comparisons in the same interface, while VisualNeuro focuses on the comparison of individual blood flow measures between two subject groups. On the other hand, VisualNeuro visually analyzes the correlation of fMRI parameters (external attributes) with neuroimaging data. This could be a useful addition to the MV^{2}Net system. VisualNeuro also presents design efforts to improve insight formation with the visual analysis tool, which could be a future work of MV^{2}Net.

2.2 Visualization for Network Comparisons

Information visualization has long been a useful way of comparing multiple data objects. In the work by Gleicher et al. [4], they summarized the visual designs for comparison into three categories: juxtaposition, superposition, and explicit encodings. Four considerations for deciding the visual comparison design are then studied, including the determination of targets for comparison, the visualization challenge, the solution strategy, and the actual design [35]. Their framework provides a unified view for both existing and subsequent visual comparison designs, in domains ranging from model comparison [36] to image analysis [37].

On comparing brain networks, all the three design categories (i.e., juxtaposition, superposition, explicit encoding) have been applied [15]. A lot of existing works studied the comparison between brain networks of individual subjects [38] [39]. More related literature compared groups of brain networks, e.g., diseased subjects v.s. controls [29], and between patients in resting-state and performing certain cognitive task [40]. Fujiwara et al. displayed each brain network as a point in the MDS projection view [40]. Users could select the networks of separate groups in the MDS view and show a detailed comparison in the correlation matrix and 3D graph views. Shi et al. proposed juxtaposed designs for group-level brain network comparisons [41] [42]. Machine learning algorithms are integrated with their techniques to conduct multivariate feature analysis on groups of brain networks.

Though comparative visualization methods have been applied extensively, most of them compare between brain networks of individual subjects or two subject groups. Few consider the visualization of correlations and trendings among related comparisons, e.g., ordered subject groups for disease progression. Furthermore, automatic analysis methods have been conducted together with existing visual comparisons. None of these methods is able to present both classical univariate analysis results and the output of multivariate testing using modern machine learning algorithms.

2.3 DTI Data Visualization

Visualizing diffusion tensor imaging (DTI) data has attracted considerable scholarly attention in scientific visualization literature. Various visual representations have been proposed, including glyphs for tensor fields [43], streamline and stream surfaces for the major eigenvector field of DTI [44], and hybrid visualization of streamlines and contextual isosurfaces [45]. To further visualize the uncertainty in fiber bundles, Brecheisen et al. [46] proposed an illustrative approach to visualize the confidence interval using the outlines and silhouettes of fiber bundles.

Most recent approaches focus on measuring similarities between fibers so that they can be clustered to reveal patterns in a concise manner. Ding et al. proposed the mean Euclidean distance for fiber clustering [47]. Physical and geometric parameters, including mean diffusivity, curvature, and torsion, were used to quantify the resulting fiber bundles. Corouge et al. compared three different metrics for clustering, including closest point distance, mean of closest point distance, and Hausdorff distance [48]. Brun et al. mapped the fibers into a feature space and constructed a similarity graph [49]. The fibers were then divided into groups using a normalized cuts algorithm. Moberts et al. proposed an evaluation framework for the different distance measures based on the correctness and completeness of clustering results [50]. Jiannu et al. used the weighted normalized sum of minimum distances to measure the similarity, favoring points with closer distances [51]. Jalba et al. constructed watershed trees to describe the hierarchy in DTI data based on log-Euclidean metric [52].

Other than the pointwise proximity of fibers, researchers also proposed to analyze DTI data in feature spaces. Brecheisen et al. designed multiple coordinated views to select and view the fibers in spatial and feature spaces [53]. Wang et al. embedded the DTI fibers into a common space so that multiple data sets could be compared in the embedded space using heatmaps [54]. Chen et al. evaluated the use of different colormap strategies in displaying 3D structural connectivity with DTI visualizations [55]. Hurter et al. proposed FiberClay, a visualization system to display DTI fiber tracts in immersive environments [56].

Most DTI visualization techniques use pointwise distance to group brain fibers for further analysis. However, the pointwise distance reflects a combined difference of multiple factors, such as spatial proximity, shape, and complexity. It does not allow the effect of each individual factor to be studied. Therefore, these techniques may not explain the role played by each individual factor.

3 MV^{2}Net: Overview

3.1 Problem Background

The neuroimaging techniques related to human brain networks are structural and functional MRIs. The structural MRIs measure the physical connectivity among brain regions by white matter pathways (i.e., brain fibers), while the functional MRIs reveal the correlation among neuronal activations of brain regions when human subjects undergo certain cognitive tasks. For the data source available in our research, we focus on the structural brain network. The structural brain network (abbreviated as brain network unless otherwise noted) is modeled by anatomical regions of cerebral cortex in the brain, known as nodes of the network; and the white matter fibers among these regions in the form of clusters of axons, known as edges of the network. Each brain region is often called an ROI and is aligned in all subjects of the same cohort. White matter fibers among ROIs are estimated from diffusion-weighted MRI, most often DTI [57].

In this paper, we target a common yet critical scenario related to the analysis of human brain networks – the detection of white matter bio-markers of certain neurological diseases, notably AD.

In general, analysts partition the derived brain networks into two groups, the diseased and the healthy (control). They are compared to extract brain connectivities relevant to the disease. Literature in the recent decade from both neuroscience and computer science have reported quite a few disease-related white matter bio-markers and have validated these findings in clinical settings. For example, it was found that AD patients underwent certain breakdown of fiber connections in frontal, temporal, parietal lobes, and posterior cortical regions of the left human brain [58] [59] [1].

Different from most existing techniques on human brain networks, we consider the uncertainty issue of underlying neuroimaging data. Data uncertainty, generally defined as the incomplete, noisy, and inconsistent nature of real-world data [60], often makes data values deviate from the correct, intended, or original values. In this work, we define the data uncertainty as the feature mismeasurement on human brain connectivity that could affect the accuracy of the targeted analysis task, i.e., the detection of bio-markers on brain connectivity. This data uncertainty can be caused by a few factors. Primarily, the same node (ROI) on brain networks of separate human subjects can refer to mildly different cerebral cortex regions. It is because the structure of the cerebral cortex can be slightly diversified across subjects. The registration of an individual subject into the same brain template often leads to deviated cortex-node mapping from the template brain cortex. Meanwhile, other factors such as the parameter and method choice of fiber tracking algorithms in brain tractography can also become the source of uncertainty in brain connectivity feature measurement. The direct impact of this uncertainty is the inaccurate task performance by our technique for two reasons. First, the p-value computed on the connectivity features can be biased because the uncertain data is included in the analysis. False-positive bio-markers can be extracted. Second, the visualization showing the average connectivity feature value of a subject group for comparison can be biased, which leads to wrong insight obtained by end users.

3.2 Pilot Study and User Requirements

The main motivation of this work lies in two hypotheses that, beyond the classical brain network visualization design with a single edge weight of connectivity strength, the visual comparison on multiple connectivity features (e.g., geometric and diffusion) of brain networks can discover useful bio-markers more comprehensively. Also, the neuroimaging and brain network construction process is noisy. The visual analysis tool on structural brain networks should be aware of the uncertainty of their data.

To validate our hypothesis and clarify the research problem of brain network comparison, we conducted pilot studies with three domain experts. The first expert was a doctor from the department of neurology in a hospital. He has both clinical and research responsibility and focuses on white matter diseases. The second expert was a neuroscientist whose doctoral thesis analyzed white matter tracts from neuroimaging data. He was previously in the ADNI team whose data was used in this work (see more details in Section 4.1). The third expert was a computer scientist whose research interests include brain network visualization and analysis. All three experts have 10+ years of experience in relevant areas of neuroscience or computer science.

The study started from a training session when the experts were communicated about the goal of this research. Next, we explained to the experts about the data source and network construction method applied. In the formal study session, each expert responded to a questionnaire and also gave verbal feedback for any extension to their answers. The questionnaires and answers are documented in Appendix A. By synthesizing the pilot study result, we summarize key user requirements on the domain of multi-variate brain network comparison.

R1: Eliminate uncertainty in brain connectivity data. The neurology doctor in our study described the comparison of structural brain connectivity as an infrequent scenario in their clinical practice. The key reason is attributed to the uncertainty of the brain connectivity data and the follow-up brain network construction process. The neuroscientist and computer scientist echoed the same uncertainty issue. They demand analyzing valid brain network data that faithfully represents brain connectivity.

R2: Analyze brain connectivity from multiple perspectives. All experts agree that the reconstructed fiber tracts represent full details of brain connectivity, much better than the brain network with a single edge weight of connectivity strength. For example, in a typical pathological disorder of brain tumors, the tumor in the early stage can cause geometric changes to the brain fiber, but without reducing the fiber connectivity strength. The analysis of brain connectivity should be conducted from multiple perspectives, on diffusion features at the voxel level and on geometric features representing the physical shape of fiber tracts.

R3: Detect brain connectivity bio-markers by statistical tests. The clinical practice to detect connectivity bio-markers for disease depends on manually spotting the difference with the naked eye, which is subjective and error-prone. Statistical tests and machine learning algorithms can detect individual connectivity features and a group of correlated features that are statistically significantly different between the comparing subject groups. Domain users demand directly looking at the analysis result instead of analyzing the raw data themselves.

R4: Iteratively compare multiple subject groups and synthesize results from multiple comparisons. To identify unique connectivity bio-markers associated with a particular disease type, neurology doctors often not only compare the group of patients having this disease type with the healthy controls, but also compare the patient group having the other type of disease with controls, and compare between the patients with different disease types. The patient groups with changing severity of disease are also compared with the healthy controls to understand the disease progression.

3.3 Visual Analytics Tasks and Techniques

To meet domain user's requirements, we design a visual analytics system namely MV^{2}Net which supports the following tasks on bio-marker detection from human brain networks. These tasks correspond to key visual analysis problems studied in this work. Several techniques of MV^{2}Net on brain network analysis and visualization are proposed to address these problems.

T1/P1: Visual quality analysis on connectivity features of the brain network. To meet R1 using visual analytics techniques, the MV^{2}Net system is designed to conduct built-in quality analysis on brain network connectivity data. A carefully engineered anomaly detection method is applied to compute the pre-defined feature quality measure. Null connections and possibly mismeasured connectivity features are assigned zero or low feature quality. More details of the feature quality analysis can be found in Section 4.2. On visualization, an interactive data wrangling mechanism is designed and implemented to allow users to eliminate the data uncertainty before the network comparison analysis (Section 5.2).

This article has been accepted for publication in a future issue of this journal, but has not been fully edited. Content may change prior to final publication. Citation information: DOI 10.1109/TVCG.2021.3098123, IEEE Transactions on Visualization and Computer Graphics

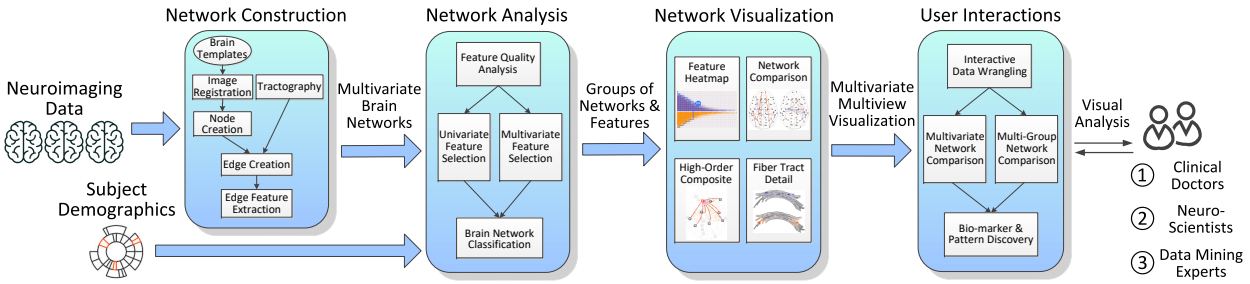

Fig. 1. The visual analytics pipeline of MV^{2}Net composed of brain network construction, analysis, visualization, and interaction stages.

T2/P2: Visualization of discriminative connectivity features between two groups of brain networks (univariate bio-markers). To achieve R2 and R3 on individual connectivity features, the system integrates univariate statistical tests (e.g., the Student's t-test) with interactive brain network visualization (Section 5.3). Multiple choices of statistical test algorithms and visual comparison modes are supported in the system. Users can directly manipulate the algorithm parameters and visually analyze the outcome. A visual interface for subject group selection is also introduced to specify the comparison setting.

T3/P3: Visualization of correlated discriminative connectivity features between two groups of brain networks (multivariate bio-markers). The system also satisfies R2 and R3 on correlated connectivity features, e.g., multiple discriminative features on the same brain connection, or the same feature on a subgraph of the brain network. Multivariate feature selection algorithms are applied to extract discriminative subgraph features (Section 4.3). A high-order composite visualization design is introduced to analyze correlated connectivity features on the same brain connection (Section 5.4).

T4/P4: Visual analysis of multiple group-based brain network comparisons. To meet R4, MV^{2}Net visualization is designed with multiple comparison views (Section 5.3). Both correlation and progressive patterns in these comparisons can be visually detected. Composite visualizations are also supported to integrate the multiple comparisons into the same view for analysis. To allow users to examine bio-markers on low-level connectivity, a 3D comparison view is provided to drill down to detailed geometric/diffusion features on the fiber tract level (Section 5.5).

3.4 System Pipeline

We implement MV^{2}Net by a pipelined system architecture, as shown in Figure 1. In the first stage, raw neuroimaging data of all subjects are registered into the same brain space to create brain networks that are comparable with each other. Multiple connectivity features are extracted for the multivariate network analysis in the second stage. Both univariate and multivariate discriminative features are selected to accurately classify brain networks according to their diagnostic or demographic groups. The main innovation of this work lies in the elaborately designed and coordinated visualizations on feature distribution, network comparison/composition, and fiber tract details. Users are allowed to interact with visualization in multimodal methods, which helps to fulfill their ultimate task of detecting bio-markers and brain network patterns for neurology diseases.

4 Brain Network Analysis

4.1 Multivariate Brain Network Construction

We developed MV^{2}Net system mainly using the data set from the Alzheimer's Disease Neuroimaging Initiative (ADNI) – a public Consortium on collecting, validating, and utilizing AD data [61]. The ADNI data set contains structural MRIs of 202 subjects recruited and scanned at 16 different sites across North America [1]. On each subject, we computed a structural brain network by the segmentation method distributed with the FreeSurfer tool [62]. FreeSurfer applied the Desikan-Killiany parcellation template [63], which defines 70 ROIs (nodes) on the brain cortex of each subject. The default edge weight between two ROIs is set to the number of fibers on the white matter pathway between them, estimated from the DTI data of each subject.

Motivated by the user requirement to comprehensively understand brain connectivity (R2), we extract multiple diffusion and geometric features from the white matter pathway among ROIs, together with the connection strength (#fibers) commonly used as the edge weight in brain networks. Existing literature have demonstrated the linkage between diffusion features and neurological pathology [29] [64]. We selected four most popular DTI metrics as diffusion features analyzed in the system, namely fractional anisotropy (FA), mean diffusivity (MD), axial diffusivity (AxD), and radial diffusivity (RD). Meanwhile, it is also believed by experts in our pilot study that certain neurology diseases can be correlated with the change in geometric features of the subject's brain white matter pathway, with or without affecting the connection strength of these pathways. We consider four geometric features in our current implementation: namely, length, curvature, torsion, and entropy. We use the length, curvature, and torsion, as they precisely describe the spatial patterns of brain fibers. We use the length and entropy, as they partially reflect the reliability of the fibers. The DTI images are often suffered from uncertainties, which makes the longer fibers or fibers in complicated regions less reliable. By considering these four features, we incorporate the information of white matter pathways in multiple aspects, aiming for a more comprehensive analysis than using the single metric of connection strength (Figure 2(a)).

In more detail, the last three geometric features are uncommon to the community of network analysis. Fiber curvature indicates the amount of fiber deviated from being straight at any point of the fiber. As shown in the lower part of Figure 2(c), the red point where the fiber can accommodate a bigger circle has a lower curvature, while the blue point accommodating a smaller circle has a higher curvature. Fiber torsion indicates how sharply the fiber is twisting out of the plane of itself. In the spring example at the lower part of Figure 2(d), the points in the stretched part of the spring have higher torsions, while the points in the compressed part have lower torsions. Both curvature and torsion of a fiber are computed by the

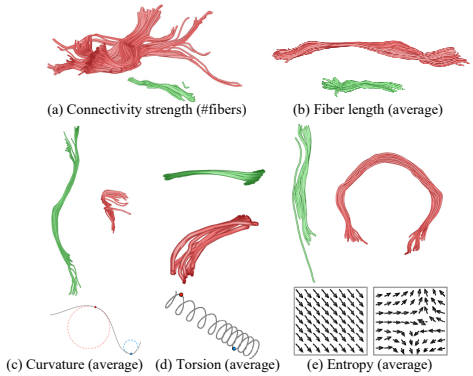

Fig. 2. Five geometric features used in MV^{2}Net (including connection strength). The fiber bundle in red indicates that these fibers have larger values on the corresponding feature in comparison to the fiber in green.

average feature value at all points on the fiber. Finally, fiber entropy measures the degree of disorder in the orientations of a fiber. In the left part of Figure 2(e), the fibers close to straightlines have narrowly distributed fiber orientations and lower entropies; while the fibers in the right part of the figure have the more disordered distribution of orientations and higher entropies.

To compute the diffusion and geometric features of a white matter pathway between two ROIs, individual brain fibers are first tracked by the tractography algorithm [65] over the DTI data. Next, diffusion and geometric features are computed on each voxel (FA/MD/RD/AxD/curvature/torsion) or fiber (length/entropy), and then averaged on the set of fibers belonging to the white matter pathway. Finally, the multivariate brain network is formed by the multiple features estimated on each edge. Besides the brain networks inferred from MRIs, ADNI data also comes with demographic information of subjects. Each subject has a diagnosis class. There are 50 healthy controls, 72 early MCI (eMCI), 38 late MCI (lMCI), and 42 AD patients. Additionally, the subjects are also recorded with their gender (82 females, 120 males) and age group (55 to 90 years).

4.2 Feature Quality Analysis

To solve the visual analytics problem of analyzing data uncertainty on multivariate brain networks (P1), we propose an interactive method to allow users to decide on the scope of feature comparison for bio-marker detection. A measure of feature quality for brain network comparison is first defined, which is called Quality for Comparison (QoC in short). Then we introduce the quality analysis method based on the QoC measure. In our method, zero feature values are assigned the zero quality, indicating null connection features. For non-zero feature values, those features statistically deviated from the feature value distribution are assigned low qualities.

On the connectivity features extracted in Section 4.1, it is found that the feature distributions largely follow normal distribution after removing zero values. Therefore, we apply the parameter-free Grubbs's test as the anomaly detection algorithm to extract zero-quality outlier feature values and compute the QoC measure for the other feature values. The Grubbs's test adapted to our quality computation usage is given below. More details of the QoC measure and its computation algorithm can be found in Appendix C.

Consider a data set of N subjects, denote the value of the jth connectivity feature on the ith subject by x_{ij}. On the jth feature, the Grubbs's test first computes a test statistic by

$$G_j = \frac{\max_{i=1,\ldots,N} \left| x_{ij} - \bar{x_j} \right|}{s} \tag{1}$$

where $\bar{x_j}$ and s denote the sample mean and standard deviation of value distribution on the jth feature.

The critical value of Grubbs's test under the current data size (N) and significant level (α) is defined by

$$H_N(\alpha) = \frac{N-1}{\sqrt{N}} \sqrt{\frac{t^2_{\alpha/(2N),N-2}}{N-2+t^2_{\alpha/(2N),N-2}}} \tag{2}$$

where $t_{\alpha/(2N),N-2}$ denotes upper critical value of t-distribution with $N-2$ degrees of freedom and a significance level of $\alpha/(2N)$.

In case the current test statistic is larger than the critical value ($G_j > H_N(\alpha_{min})$), the most deviated value is classified as an outlier and assigned a QoC measure of zero. The outlier is then removed from the distribution and the Grubbs's test is repeated until no outlier can be found. Here α_{min} denotes the significance level used for the Grubbs's test and is set to 0.05 by default.

After the Grubbs's test, the QoC measure of remaining values on the jth feature is computed by the following mapping function in a decreasing order without removal:

$$q_j = \max(0, 1 - \frac{\log H_N^{-1}(G_j)}{\log \alpha_{min}}) \tag{3}$$

The quality of feature values is visualized in the heatmaps of MV^{2}Net. As shown in Section 5, more than a half feature values on some connectivity could be outliers (zero quality). The quality analysis helps to improve the fidelity of visual discovery by interactively filtering outliers out (Section 6).

4.3 Discriminative Feature Selection

To address the visualization problem in displaying discriminative connectivity features (P2 and P3), we apply both univariate and multivariate feature selection algorithms in MV^{2}Net to identify connectivity features that are significantly different between the brain networks of contrasting subject groups. The univariate algorithm introduces a statistical hypothesis test on each connectivity feature of the network. Under the normality assumption verified in Section 4.2, the Student's t-test is legitimately used, which computes a p-value on each feature. When the p-value is no greater than a significance level (0.05 by default), the mean feature values of two contrasting groups on the corresponding feature are said to be significantly different. These selected significant features will be visualized in MV^{2}Net for further analysis. Note that when the feature variance of contrasting groups is unequal, the Welch's t-test can be applied instead of the standard t-test. Users are allowed to choose between the two tests for every comparison.

According to clinical researches on white matter disorder, there are two major types of brain connectivity destruction: one on a certain scope of white matter that mostly affects a single brain network connection; the other on a range of cerebral cortex spanning multiple ROIs (mainly grey matter) that could affect all brain fibers connecting to these ROIs. In the latter case, the connectivity features associated with affected ROIs will be correlated in the diseased subjects, e.g., with decreased connectivity strength simultaneously. Yet, each individual connectivity feature may not be significantly different between the comparing subject group. The univariate feature selection algorithm will not solve the

problem in this case because it analyzes each feature independently. Lowering the p-value threshold also does not work as this will produce too many discriminative features without detecting the feature correlation. We consider the multivariate feature selection method called group lasso (GL), which is a kind of supervised machine learning algorithm. The algorithm aims to leverage the supervision to guide the selection process for a subset of discriminative features, instead of extracting a single feature in the univariate analysis. The method takes both connectivity features and the brain network structure as input. A set of structurally correlated connectivity features (e.g., on the subgraph of brain network) are then detected. When applied collectively, these features can precisely predict the subject label of a brain network, i.e., patient or control. The prediction accuracy is displayed in the interface to demonstrate the performance of the model. To evaluate the significance of each of these multivariate features, we apply univariate statistical tests on each feature and display the derived p-values in the interface for the visual analysis of multivariate bio-markers.

The details of the adaptation of the GL algorithm in our system are described below. First, all brain network connectivities are partitioned into blocks via ROI clustering. Second, the GL model on two contrasting subject groups is formulated and solved over these connectivity blocks. Third, the selected features by the GL model are processed again by statistical hypothesis test and regression analysis to compute performance indicators for visualization (i.e., p-value and classification accuracy). The objective function of the GL model is given below.

$$Minimize \sum_{i=1}^{N} log(1+e^{-y_i W^T X_i}) + \lambda \sum_{m=1}^{M} ||W^{(m)}||_2 \qquad (4)$$

where N and M are the numbers of subjects and feature groups. $X_i = (x_{i1}, \cdots, x_{iR})'$ denotes the vector composed of all the R connectivity features on the ith subject, $y_i = \{1, -1\}$ denotes the outcome category of the ith subject (e.g., AD or control). $W = (w_1, \cdots, w_R)'$ denotes the vector of regression weights for the features, $W^{(m)}$ is the partial weight vector of the mth feature group. The parameter λ controls the degree of sparsity. The feature with a larger weight indicates that it has a higher influence on the prediction of subject groups. The GL model explicitly combines two types of terms: the Negative Log Likelihood (NLL) of a logistic regression model, and L2-norm regularization terms for each feature group. The NLL term stresses the predictive power of the model, while the regularization term shrinks the components in the weight vector W towards zero in a group-based manner to achieve feature selection.

In determining connectivity feature groups ($W^{(m)}$) for GL models, we apply ROI clustering instead of the direct connectivity grouping, as it is hard to estimate the spatial distance among multiple fiber connections (mostly twisted together). While more sophisticated clustering algorithms can be designed, we stick to two anatomical ROI grouping methods when the number of ROIs in the brain is sufficiently small (70 in this work). In the first method, we let each ROI be a single cluster; in the second method, ROIs are grouped into 12 lobes in two hemispheres according to the lobe classification of the human brain [66]. Finally, each ROI cluster is expanded into a block of connectivity features affiliated with any ROIs in the cluster. Each feature is duplicated into two copies for its starting and ending ROI clusters respectively since the brain network is undirected. The blocks of features are then fed to the GL model. The algorithm-selected features are visualized in the comparison view, showing three importance metrics: the feature weight computed in the model which infers its importance to the predictive model, the original p-value indicating its discriminative power, and the prediction accuracy as a block of features together. Note that the p-value of each feature in multivariate comparison is the same as the p-value in univariate comparison, except that p-values lower than the threshold can also be displayed if they are selected by the algorithm.

5 VISUALIZATION

5.1 MV^{2}Net Interface Design and Rationale

MV^{2}Net system is built to address the visual analytics problems defined in Section 3.3. The design rationales of MV^{2}Net visualization also largely focus on solving these problems.

- **Uncertainty-aware:** The interface should allow users to understand the uncertainty of connectivity estimation in brain networks. To get rid of null or mismeasured network connectivity, users need to interact with the interface to filter out the uncertain data based on their domain knowledge and focus on cleaned data for further analysis. (P1)
- **Multi-variate:** To obtain a comprehensive overview of brain networks in the data set, users need to look at each brain connectivity from multiple extracted features. Visual comparison or correlation analysis among these multivariate features are essential for most user tasks related to bio-marker detection. (P2, P3)
- **Multi-view:** The brain network patterns revealed in different connectivity features, contrasting subject groups, and feature selection algorithms are often quite versatile. It could take users a huge visual burden to perceive and analyze these patterns in the same view. Multi-view design could help them flatten the cognitive effort into a principled visual analytics process by examining one perspective at a time. (P4)
- **Level-of-detail:** The scale and complexity of potential bio-markers in numerous comparisons of contrasting subject groups calls for a level-of-detail design in visualization. Users could first locate individual clues in separate univariate feature views, compare different features side-by-side for correlations, then validate the correlation in a more fine-grained high-order composite view, and finally drill down to the detail of identified bio-markers through 3D geometric visualization. (P2, P3, P4)

In the formalized design, users start by selecting two groups of subjects by navigating the metadata hierarchy of the data set in a sunburst visualization (Figure 3(a)). Later, s/he could come back to study another pair of subject groups in the same view. The quality of connectivity features in the selected groups are then displayed in multiple *feature heatmaps* (Figure 3(b)), where the uncertain part of data could be manually filtered out. Relevant connectivity features are picked and displayed in the *network comparison* view for both single-connection and multi-connection bio-marker detection (Figure 3(c)). Upon identification of correlated or progressively changing connectivity features, users could synthesize the finding in a *high-order composite* view to better reveal the multivariate pattern (Figure 3(d)). The detected pattern is further expanded in the geometric detail view for externalization and explanation (Figure 3(e)).

5.2 Feature Heatmaps

As shown in Figure 4(a)(b), the heatmaps illustrate the quality distribution of feature values by brain connectivity, individual

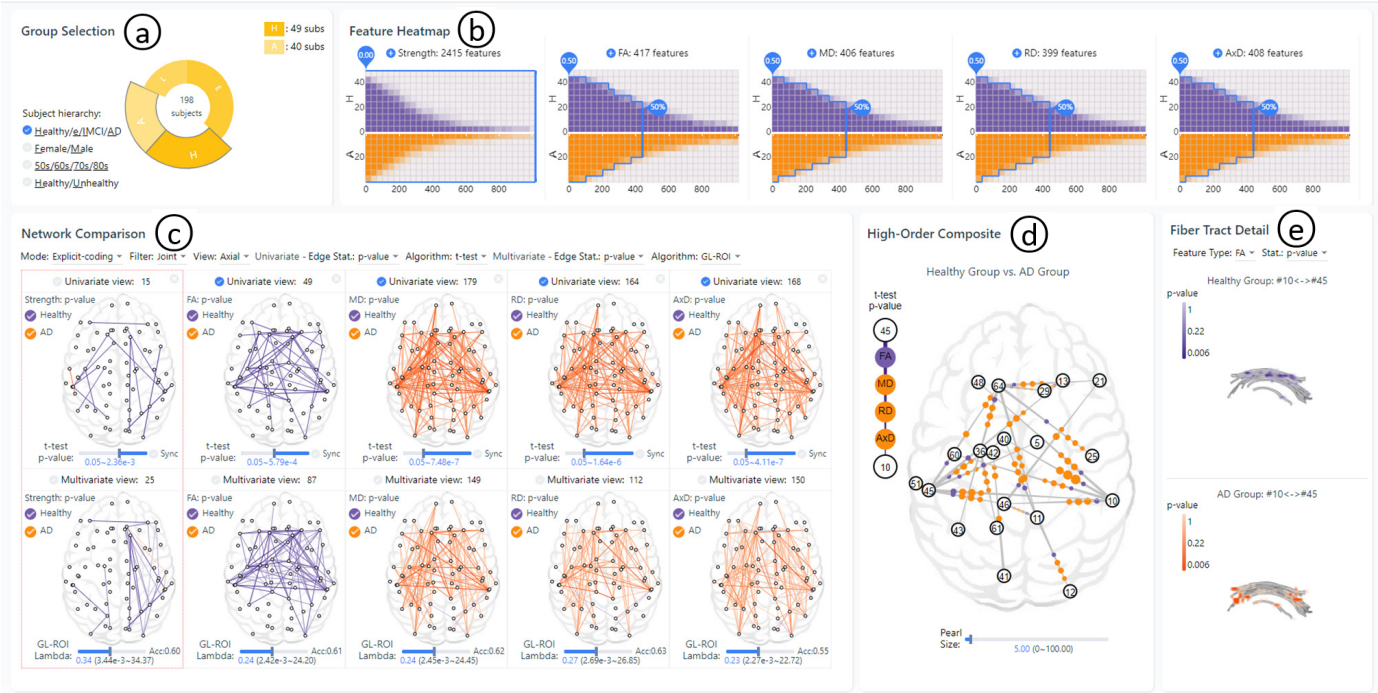

Fig. 3. The visualization interface of MV^{2}Net: (a) selection panel for two subject groups under comparison; (b) heatmaps showing data quality in the subject by feature matrices which helps to select high-quality features; (c) brain network view for group-based comparison; (d) high-order composite of multiple comparisons; (e) 3D view of fiber tract details between two selected ROIs.

subject, and feature type. Each heatmap in a sub-figure indicates a connectivity feature in strength/FA/MD/RD/AxD (diffusion features, Figure 3) or strength/length/curvature/torsion/entropy (geometric features, Figure 10). The X-axis represents ROI connections (edges) in the brain network. As we have removed all empty connections (zero feature quality in all subjects), there are less than a thousand valid connections on each feature. The Y-axis represents the subjects in our data set and is partitioned into upper (purple) and lower (orange) sides, corresponding to two selected subject groups in contrast. Each cell inside the heatmap is filled whose color saturation is linearly mapped to the quality of the corresponding connectivity feature and subject. The more saturated, the higher quality. As each heatmap with more than 100k cells is costly to render, we aggregate adjacent cells in a fixed grid setting. The aggregated cell then depicts the average feature quality of the original cells inside it. To ensure a reasonable cell aggregation, brain connectivities are sorted by the number of qualified subjects along the X-axis. The subjects in each column (connectivity) of the heatmap are sorted separately by their quality value. The smoothness of resulting heatmap visualizations demonstrates the effectiveness of cell aggregation.

To filter out uncertain data for further analysis, an interactive wrangling mechanism is designed. Each heatmap is drawn with a blue outline. The horizontal zigzag borders at the top/bottom of the outline indicate a lower bound quality threshold for both subject groups, which is set to 0.5 by default. The cells within the borders represent subjects who have qualities higher than the threshold in the corresponding connectivity feature (column). Similarly, a vertical border on the right indicates the lower bound threshold of the percentage of qualified subjects for each brain connectivity, which is set to 50% by default. Both thresholds can be adjusted through direct user manipulation of the outline. The cells within the selected outline represent user-specified qualified brain network features for comparison. Users could add these features to the network comparison view for further investigation by clicking the "+" buttons above each heatmap.

In addition, to visually explain the quality measure to users and instruct them for the feature filtering practice, we design a detailed quality visualization panel on the heatmap view. As shown in Figure 4(a)(b), by mouse hovering of any cell on the heatmap, the quality panel is shown on-demand at the upper-right corner of each heatmap view. In the panel, the probability density distribution (PDF) of all feature values within the hovered cell is displayed in green bar charts (Figure 4(a)). In the background of the quality panel, the average PDF of the same connectivity features on two comparing subject groups are drawn in purple and orange line charts respectively. They correspond to the upper purple part and the lower orange part in the same column with the hovered cell. The shaded purple/orange contours centered on the purple/orange line charts represent the variation (75% CI) of feature distributions across all subjects in the same group. The visualization result in Figure 4(b) on a low-quality cell (grey color) indicates that the distribution of low-quality feature values, as shown by the green bar charts close to zero, is significantly different from the high-quality features in both subject groups, as shown by the line charts. The difference between the high vs. low-quality features is much larger than the difference between the features in comparing subject groups.

5.3 Network Comparisons

The comparison view (Figure 3(c)) displays brain networks in contrasting groups for visual detection of bio-markers. Each column in the view corresponds to one feature added from feature heatmaps and is composed of two separate brain network visualizations. By default, the quality filter specified in the heatmap view applied to the comparison view of the corresponding feature. A joint filter option can also be used in which quality filters in all features are jointly applied in each comparison view. The joint filter allows

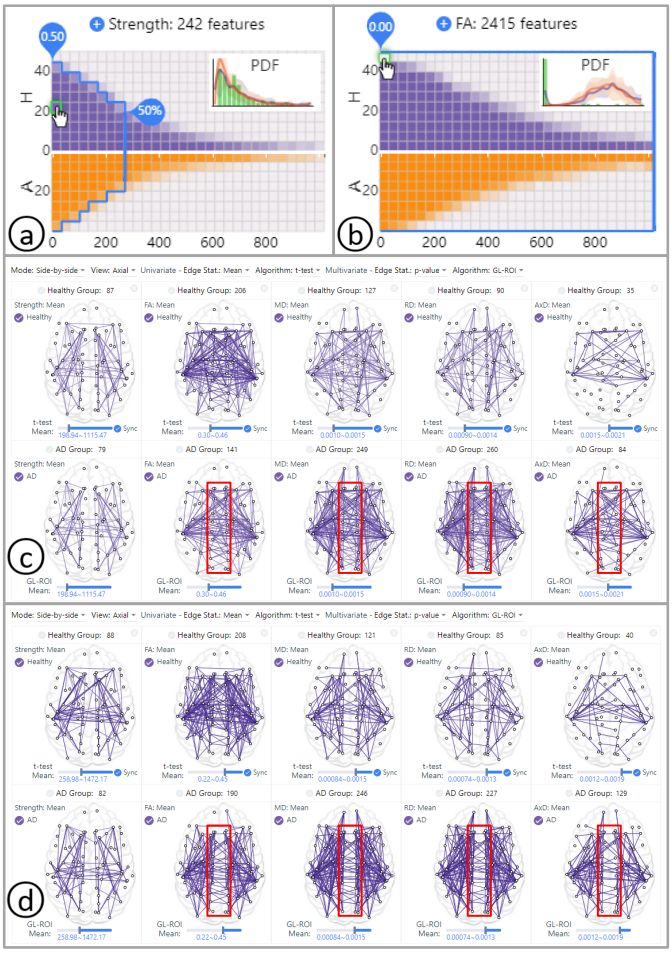

Fig. 4. Side-by-side comparison of AD patient group and healthy control group: (a) feature heatmap with the default quality filter, mouse hovering a cell with high-quality features; (b) selecting all 2415 features with filters disabled, mouse hovering a cell with low-quality features; (c) brain network comparison on selected high-quality features between the two groups; (d) brain network comparison on all features with the top average values.

invalid brain connections to be removed given indicator on one of its connectivity features. The visualization for comparison is designed into two modes which can be switched in the configuration menu on top of the view.

In an explicit-coding mode (Figure 3(c)), the upper and lower visualizations in each column display the output of univariate and multivariate feature selection algorithms respectively. Over the base graph of a human brain, network nodes are drawn by small circles at the center of each corresponding ROI. In the upper univariate view, network edges are drawn between ROIs whose color saturation displays the value of $-log(p-value)$ from the statistical hypothesis test (t-test). Here p-value indicates the significance level of feature difference between contrasting subject groups on the edge. The edges with a higher average feature value in the first group than the second group are drawn in the purple color, and the other edges are drawn in the orange color. Legends for the two types of edges are placed in the top-left part of the view and can be checked/unchecked by users to display/hide each edge type. In the lower multivariate view, the network by default displays connectivity features selected in group lasso models and can also be switched to other feature selection algorithms. Users can choose to show three different feature statistics on the network edge of multivariate view: p-value in t-test (default), feature weight by the multivariate model, classification accuracy of the same selected feature set in a regression model. In another side-by-side comparison mode (Figure 4(c)(d)), the upper and lower visualizations in the same column display the average brain network of each selected subject group respectively. Network edges are drawn to represent the selected feature statistic in the subject group. Users can choose from three statistics: average (default), standard deviation, #subject.

In both visualization modes, several user interactions are supported to optimize the bio-marker detection process. Edge connections of the networks can be pruned by tuning a slider beneath each view, which indicates the lower bound of displayed feature values. Only important connections are kept in the view to alleviate the visual complexity for analysis. Mouse-hovering on each edge will pop up the details of the connection, including source/destination ROIs and feature statistics. Among columns of brain networks, each network view can be selected by a mouse click, as shown by the visual hint of a red outline in the view. The mode, visual design, and algorithm configuration of the selected network comparison can be set in the drop-down menu.

Notably, the projection of brain network visualization can be switched among axial, sagittal, and coronal views. An optimal view point can be chosen by users to avoid the occlusion of key bio-markers. The order of comparison views in the row can be re-arranged through mouse dragging. Each view can be closed when the analysis is finished. This helps to prepare ordered inputs to the next composite view for detailed correlation analysis.

5.4 Brain Necklaces

The high-order composite view aggregates selected network comparisons to reveal the bio-marker expressed on multiple features simultaneously or the bio-marker changing progressively across subject groups. As shown in Figure 3(d), the overall design is a network visualization of ROIs, whose edges are the intersection of all displayed connections in selected comparison views. The novelty lies in a new metaphor called brain necklace that draws multiple features of the same connection as pearls on the network edge. Take the visualization in Figure 5 on one edge as an example. Each pearl is drawn as a filled circle and corresponds to one feature, with its radius and color indicating the edge feature statistics and color applied in the comparison view. To determine the order of pearls on each edge, we sort all ROIs by their degrees in the composite view. Each edge is drawn as a tapered line in grey color from the high-degree ROI to the low-degree ROI. Feature pearls are placed according to the direction of tapered lines.

There are several design choices made in brain necklace visualization. First, multiple features on an edge can also be displayed by more complex glyphs, e.g., radar charts, 3D ellipsoid. Nevertheless, high dimensional glyphs often bring a visual burden that slows the understanding of multi-feature patterns in the same view. The 3D ellipsoid is also ineffective in showing the third data dimension. On the other hand, 1D designs showing each feature as a vertical line marker or bar chart introduce visuals quite similar to the edge drawing in networks. This similarity downgrades the efficiency of pattern discovery from composite visualization.

A key issue in brain necklace visualization is the layout of feature pearls as they can heavily overlap with each other when there are a large number of edges in the composite view. We propose a distributed layout algorithm that can be computed very fast to meet the interactivity requirement in online visualization.

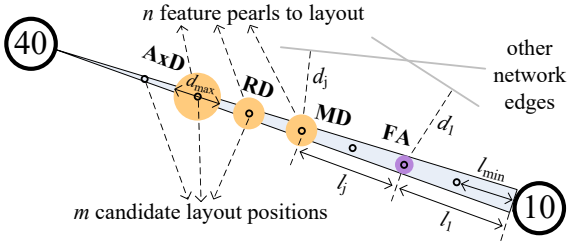

Fig. 5. The brain necklace visualization of multiple features on an edge using cost-minimization pearl layouts.

The algorithm is based on the principle of cost minimization in placing feature pearls. In detail, the cost contains two components: the overlapping cost (*cost_over*) which describes the degree of a pearl overlapping with other edges/pearls, and the spacing cost (*cost_space*) which describes the compactness of pearl placement from its previous pearl on the same edge. The costs are defined by

$$cost\_over(d_j) = \begin{cases} 0 & d_j \geq d_{max} \\ 1 & d_j < d_{max} \end{cases}, cost\_space(l_j) = (l_j - l_{min})/l_{min} \quad (5)$$

As shown in Figure 5, d_j denotes the perpendicular distance from the jth pearl (MD feature in the figure) to the closest edge other than its current edge. When this distance is large enough, i.e., small probability of overlapping, the cost is zero; otherwise, the cost is one. On the other hand, the spacing cost of the jth pearl increases linearly with the interval from the previous pearl on the same edge, denoted as l_j, excluding the minimal interval l_{min} between adjacent pearls to avoid overlaps.

The layout algorithm tries to optimize a weighted sum of the two cost components on all n pearls of an edge.

$$Minimize \quad \sum_{j=1}^{n} [(1-\alpha) \cdot cost\_over(d_j) + \alpha \cdot cost\_space(l_j)] \quad (6)$$

where α is the parameter to balance the two types of cost.

As there are infinite layout positions on an edge, we design a feasible algorithm by discretizing layout solutions. As shown by hollow points in Figure 5, we assume the pearls can only be placed in m candidate positions with a fixed interval of l_{min} from each other where $m = \lfloor L/l_{min} \rfloor$ and L is the length of the edge. The algorithm exploits a pattern in spacing cost that the cost of all pearls in an edge only depends on the position of the last pearl:

$$\sum_{j=1}^{n} cost\_space(l_j) = \sum_{j=1}^{n} l_j/l_{min} - n \quad (7)$$

Knowing that the overlapping cost of each candidate position can be pre-computed, the algorithm becomes an iteration of the position of the last pearl on the edge. For each feasible position, the overlapping cost of all pearls as well as their overall cost can be directly computed. The pseudocode of the algorithm is given in Algorithm 1 of Appendix B. Except for the pre-computing of overlapping costs, the algorithm has a linear complexity of $O(m-n)$ for each edge. Note that when an edge cannot admit n features ($m < n$), the pearls are drawn as hollow circles in the minimal size and placed uniformly on the edge.

To better analyze bio-markers from the composite view, brain necklace visualization is designed with several customized interactions. First, to reduce visual clutter, the pearls on each edge can be dragged together into more appropriate locations without re-layout. Second, users can adjust the filter on each comparison view and update the composite view instantly. Third, to focus on one ROI, users can click the corresponding node to highlight all connections of the ROI, as well as feature pearls on these edges. The other unselected edges will fade out in the background. When there are many nodes/edges in the composite view, the distributed layout result can also include severe visual clutter caused by overlapping. To reveal feature patterns clearly on the selected ROI, we introduce a distortion method on the highlighted edges. An example of the distortion result is shown in Figure 7(a)(b)(c). The technical detail is expanded in Appendix B. Finally, on the detected bio-markers, users can select the corresponding edge to show the detailed geometric and diffusion pattern in brain fiber tracts of contrasting groups in the 3D view.

5.5 Fiber Tract Details

As shown in Figure 3(e), the detail view provides a 3D visualization of brain fiber tracts on the selected network edge. The display combines tube-based visualization to draw fibers of comparing subject groups and volume rendering to display the comparative bio-marker on the fibers. For fiber visualization, we apply the technique of Merhof et al. [67] to draw all fibers in the background. For bio-marker visualization, we overlay a volume rendering of voxel-level feature statistics on the fiber tract.

Take Figure 7(d) illustrating the p-value statistics of FA feature as an example. The FA data of each subject is available at the voxel granularity from the raw imaging data. Features of multiple subjects are mapped to the same 3D space through registration. An optional smoothing step can be applied here which averages the FA value across adjacent voxels to remove noise. The t-test is then applied to the FA values of two comparing groups at each voxel. The resulting p-value will be visually displayed as the fill color saturation by the same mapping function with the other views (i.e., $-log(\cdot)$). The volume data of FA p-value is rendered by a modified version of maximum intensity projection (MIP [68]). For each pixel, we take the maximum value along the ray before reaching the opaque fibers. The use of MIP allows the largest group-level difference on voxels to be revealed. Finally, a Gaussian smoothing similar to the kernel density estimation (KDE) is applied to reduce the aliasing effect.

6 Evaluation

We conducted two case studies to demonstrate the usage of MV^{2}Net. The ADNI data set described in Section 4.1 was applied. Experts recruited in the pilot study were visited again. They were asked to use our system and evaluate its performance in meeting their requirement, e.g., comparing brain networks, detecting connectivity bio-markers for certain diseases. In the first case study, the diffusion features indicating the microstructure of brain connectivity were presented and analyzed. In the second case study, we switch to study the geometric features on the macrostructure of brain connectivity.

6.1 Case Study on Diffusion Connectivity Features

The expert started by selecting a typical comparison: 40 subjects labeled as AD patients vs. 49 subjects as healthy controls, as shown in Figure 3(a). All quality filters on diffusion features apply the default setting that accepts features legitimate in at least 50% subjects (Figure 3(b)). It can be found that most feature heatmaps have the shape of symmetric triangles. On all features, the percentage of legitimate subjects is almost the same in both subject groups. This allows us to select the same set of connection features in both groups for further comparison.

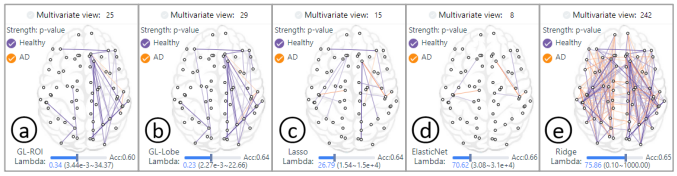

Fig. 6. The output of different multivariate feature selection algorithms in the AD vs. Control: (a) group lasso with ROI groups; (b) group lasso with Lobe groups; (c) Lasso; (d) Elastic Net; (e) Ridge.

The expert found that the diffusion features have a noticeable impact on the two groups (R2, T2). Figure 4(c) compares the healthy controls (first row) and the AD subjects (second row), where each column visualizes one diffusion feature. S/he *identified that on FA, MD, RD, and AxD, the networks of the two groups have noticeable differences,* in which the diseased group has reduced FA and increased MD/RD/AxD. The comparison on connection strength is not visually different. No asymmetric pattern between hemispheres is found in all features and subject groups.

The expert then studied the data quality (R1, T1). S/he selected all 2415 connection features in each subject's network to disable the filters (Figure 4(b)). The comparison view is updated as in Figure 4(d) where only top-valued connection features are kept so that the number of features in the healthy group is similar to the network in Figure 4(c) applying quality filters. The comparative pattern between the two groups in Figure 4(d) changes moderately from the filtered networks in Figure 4(c): on FA, it is not easy anymore to visually detect reduced network features on the diseased group. More impact of the data quality filter happens on the altered network pattern within each subject group. *The expert found that the brain network without applying quality filters has fewer connections between hemispheres as its top features (in red rectangles of Figure 4(d)).* S/he hypothesized that longer brain fibers (e.g., those between hemispheres) were less accurate to be traced by the tractography algorithm. These fibers normally have smaller average feature value due to mismeasurement in some subjects. By applying the quality filter, the uncertainty from mismeasurement is alleviated so that these fibers are visible as top features. This bias for long brain fibers also accounts for the change on comparing the FA metric. As an indicator of intactness of white matter structure, the FA metric is often reported to decline in AD patients, especially in long-range connections. Because the long-range connection is more likely to be messed with uncertain data and dropped from top features, the brain network comparison without a data quality filter will have the less significant comparative pattern on FA between AD patients and healthy controls.

The expert switched to the explicit-coding comparison mode to further examine the network difference between the diseased and control groups (R3, T2, T3). The first row in the comparison view (Figure 3(c)) now displays the univariate t-test result on each connection feature. The p-value threshold is set to 0.05 for all views so that the displayed connection features will have significantly different values between the two subject groups under comparison. The visual evidence confirms that the diseased subject group has reduced FA statistically, as shown by the dense purple connections in the second column of the view. MD/RD/AxD have increased from the control group, as shown by the orange connections in the last three columns. The second row in the comparison view (Figure 3(c)) showing the result of multivariate feature selection mostly reveals a similar comparative pattern to the output of t-test in the first row. *Notably, on the strength feature, the multivariate algorithm detects a set of discriminative connection features in the left hemisphere (right part in the axial view) on which the AD group has decreased connection strength. This suggests a potential asymmetric effect of AD disease on human brains.* The expert also investigated multivariate comparison using different feature selection algorithms. As shown in Figure 6, the two algorithms exploiting the natural grouping of brain connections detect a similar asymmetric pattern ((a) and (b)), while the other three algorithms without feature group information detecting much fewer discriminative features scattered in the whole brain ((c)(d)(e)). The result supports the use of group lasso as the default multivariate feature selection algorithm in our system.

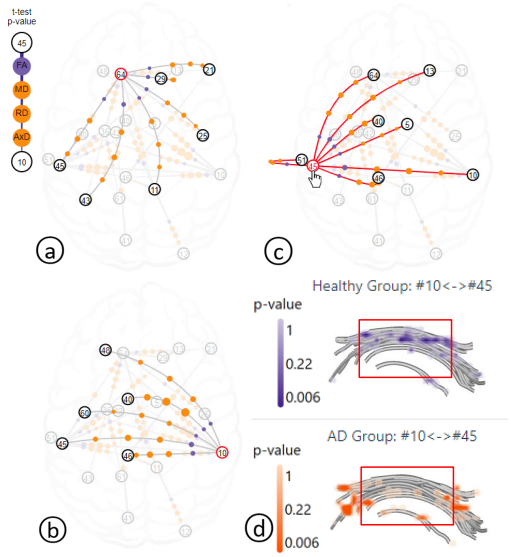

Fig. 7. The composite view showing the correlation of comparison result on four features (FA, MD, RD, AxD): (a) ROI #64; (b) ROI #10; (c) ROI #45; (d) fiber tract detail of ROI #10∼#45.

The expert stated that the above findings on the comparison of AD and control groups correspond well with the clinical explanation of DTI metrics in the literature. FA is known to represent the integrity of white matter [69]. The value of FA drops as the white matter of the human brain suffers from progressive damage during AD. MD captures the average rate of diffusivity in all directions and will increase with white matter damage as the microstructural barrier for water diffusion is alleviated [64]. RD also increases because of the demyelination effect associated with AD [70]. AxD was reported to increase with white matter neurodegeneration, but the clinical base of the correlation is still to be discovered [71]. Meanwhile, the asymmetric impact of AD on brain connectivity has also been found previously in DTI data analysis [1] and clinical study [72].

The expert further drilled down to the details of brain connectivity change for AD patients. On the detected difference of FA, MD, RD, and AxD features in Figure 3(c), s/he aggregated univariate comparison of the four features into a high-order composite view (Figure 3(d)) (R2, R3, T3). *In the composite view, the expert identified three ROIs with many connections showing significant differences on all the four features: ROI #64, #10, #45.* Their connections and feature differences are revealed in Figure 7(a)(b)(c) respectively. The expert also aggregated multivariate views and obtained similar results. Among these discriminative features, the connection between ROI #10 and #45 was found to have the most significant difference on FA, as shown by the largest purple pearls in Figure 7(b). *The voxel-based comparison further reveals the detailed difference (Figure 7(d)).* The expert found that several

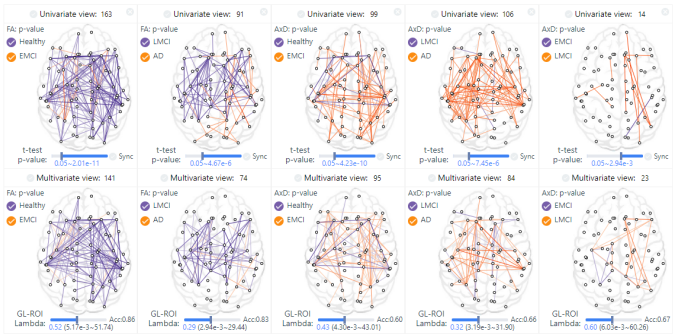

Fig. 8. Brain network comparison among multiple diagnostic groups for the analysis of AD progression.

segments of the fiber tract have reduced FA in the AD group, as shown by the purple regions in the upper sub-view. These regions locate on intermediate parts of the fiber tract (in red rectangles), in comparison to orange regions at endpoints of the fiber tract in the lower sub-view, which indicate increased FA in the AD group. After an examination of fiber anatomy in human brains, it is found that the intermediate segments of the fiber tract between ROI #10 and #45 are part of the corpus callosum. The detected bio-marker conforms with the clinical evidence that corpus callosum progressively degenerates with decreased white matter integrity during the onset of AD [73].

The detected individual bio-markers on ROI can also be traced back to clinical evidence. In early research of AD [74], certain types of pyramidal neurons were reported to be lost in the superior frontal (#64) and inferior temporal (#10 and #45) cortex. This pathological change could diminish the effectiveness of distributed processing capacity of the neural cortex. The superior frontal gyrus was reported to have cortical synaptic loss and inflammation in AD patients [75]. The synaptic loss was also observed in the inferior temporal gyrus of AD and MCI subject groups [76]. The synaptic numbers highly correlate with the Mini-Mental State Examination (MMSE) score, which is a widely-used test for assessing cognitive function among the elderly. Several other pathological changes were also found in the superior frontal or inferior temporal cortex of AD patients, including reduced metabolic rate [77] and increased lipid peroxidation [78].

After the comparison of diseased and healthy subject groups, the expert followed up to study the progression of AD by comparing subject groups in four stages of the disease (R4, T4). The visualization interface of MV^{2}Net enables users to juxtapose several group comparisons to understand the progression of brain networks on an ordinal attribute of subjects. As illustrated in Figure 8, the change of brain connectivity on FA and MD/RD/AxD is found to be similar to the change from healthy controls to diseased subjects, in a direction from controls to eMCI and from lMCI to AD patients. The result is consistent with the well-known progressive nature of AD. In the first two columns of Figure 8, the FA metric is reduced during the progression. *The decrease of FA firstly happens more in the left hemisphere (control to eMCI), and then happens more in the right hemisphere (lMCI to AD).* The asymmetric progression of AD was previously reported in clinical studies that pathological changes appear earlier in the left hemisphere than in the right [72]. Meanwhile, MD/RD/AxD have largely increased feature values, with the example of AxD in the third and fourth columns of the figure. Notably, the network comparison between eMCI and lMCI subjects shows little difference, as illustrated in the last column of Figure 8 (AxD). The less distinguishable eMCI/lMCI comparison is

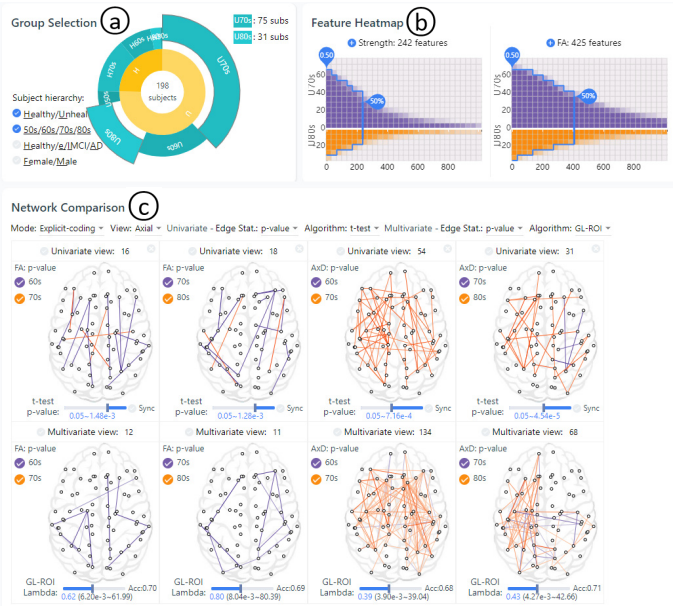

Fig. 9. Brain network comparison among multiple age groups.

not surprising, as the ADNI data set applied in this work originally only has one MCI class (lMCI here). The eMCI class is created later and secondary to the control/MCI/AD classification [79].

The expert also studied the progression of brain network changes among age groups of our subjects (R4, T4). Because 95% subjects in our data have ages between 60 and 89, we partitioned the data into three age groups for the analysis: 60∼69, 70∼79, 80∼89. Figure 9 indicates that aging seems to be a similar factor to AD leading to the breakdown of brain connectivity, as shown by the result on FA and AxD in the first two and last two columns of the figure. However, the impact of aging is much smaller than the disease. *The number of significantly changed individual connection features in the age progression of Figure 9 is less than one-third of that in the disease progression of Figure 8.* The age progression is especially milder on the FA metric. This result suggests that the AD disease causes more noticeable and independent consequences in the brain network than normal aging [80]. The impact of other factors (e.g., gender) on the brain connectivity was also examined by the expert. Nevertheless, *none of these factors interfere with the detected pattern of connectivity break-down in AD patients, as well as the progression with disease and aging.*

6.2 Case Study on Geometric Connectivity Features

We apply the same system to the geometric features extracted from brain connectivity data. Our findings from the study are quite different from the result on diffusion features. Figure 10 gives the visualization comparing AD and control groups with the default data quality filter. It can be found that while the data quality distributions of these geometric features (Figure 10(a)) are quite similar to diffusion features (Figure 3(b)) (R1, T1), *very few significantly different connection features can be detected between the two subject groups.* The univariate views in Figure 10(b) mix both connections larger in the AD group and connections larger in the control group with only a few synchronized connectivity patterns among the four features (R2, R3, T2).

The progression of AD and aging effect on geometric features is also explored by the expert (R4, T4). *No consistent progression pattern on brain networks is found across diagnostic groups and age groups for all geometric features.* Figure 11 displays the result

Fig. 10. The MV^{2}Net visualization comparing geometric features of the brain network between the diseased group and the control group.

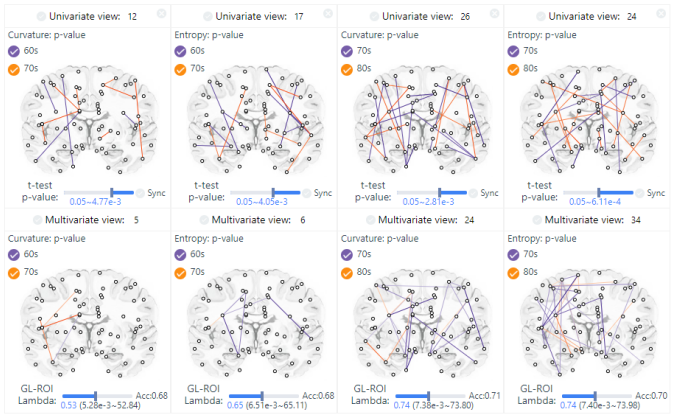

Fig. 11. Brain network comparison among multiple age groups on geometric connectivity features.

comparing three age groups. Only a few significant changes are detected, without a clear pattern favoring older or younger groups.

The smaller impact of AD on the macrostructure of brain connectivity seems to be reasonable as most existing literature on pathological bio-markers of AD point to the microstructure of brain connectivity, particularly revealed by diffusion metrics of DTI data. The only affected macroscopic measure, namely connection strength, is computed from the 3D field of FA, which highly correlates with the microstructure of brain white matter. The metric of connection strength is also less significant as AD bio-markers than microscopic metrics such as FA and MD.

In summary, the case study result demonstrates the unique capabilities of our system in comprehensively comparing human brain connectivity and detecting effective bio-markers, which are not possible with previous visualization tools. First, it is shown that in real-world data, comparing brain networks on a single connectivity feature (strength or FA) is insufficient. Many diffusion-feature bio-markers are found in our system by synthesizing the group difference on multiple features. Second, through experiments with and without a data quality filter, we prove that data noise and outlier can make a major impact on the distribution of brain connectivity, which is hardly considered in the literature. Our system eliminates these illegitimate data by an interactive data wrangling mechanism. Third, our system allows the incorporation of new brain connectivity features in the visual comparison process. For example, the geometric connectivity features are extracted, analyzed, and visualized in our system. As shown by the case study result, very few of these geometric features are discriminative between neurologically diseased people (e.g., AD) and normal controls. This finding somehow updates the experts' knowledge that the geometric features could be useful in the connectivity comparison (see Appendix A about experts' answers on geometric features in the pilot study).

6.3 Expert Feedback

After the pilot usage, experts were asked to respond to several questions regarding the current functionality and potential extension of MV^{2}Net, as well as providing open comments. On the positive side, the experts described the system as comprehensive. While their previous approach analyzed brain connectivity in a (diffusion) feature by feature, fiber (pathway) by fiber, and (subject) group by group basis, our system could bring these pieces together and connect the dots to disclose additional information to the current knowledge of Alzheimer's disease. This is also shown in the case study. On the constructive side, several new design features were mentioned in their feedback. For example, they required a display of top-10 connection differences on certain features and the description of these connections, so that users could know what they are. They suggested integrating the brain network anatomy of normal people so that the networks of both diseased subjects and controls can be calibrated for bio-marker detection. The experts also proposed to allow different kinds of neuroimaging data input, either on Parkinson's disease, encephalitis, or from new cohorts as the ADNI study continues. It was mentioned that certain neurology diseases such as encephalitis are treatable, which is unlike the irreversible progression of AD. The brain connectivity of patients can recover as they are being treated. Our system showing the multimodal connectivity of human brains can be a useful tool for assessing the state and progress of this treatment.

In the verbal feedback, the neuroscientist who shares the experience in analyzing ADNI data provided more detailed comparisons between MV^{2}Net and his previous workflow. As described in Jin et al. [29], their framework focused on clustering individual fibers from the DTI data into major tracts, and developed a novel method to extract discriminative diffusion features between the subject groups under comparison. On visualization, they applied existing imaging tools which can only display a single feature between two comparing groups under a pre-defined parameter set at a time. They commented our system to have more options and information in visual comparison, including the support of many connectivity features in the same interface with multiple views, the interactive manipulation of algorithm parameters, and the direct display of comparison results. On the approach to directly visualize the p-value of statistical test results, the neuroscientist and computer scientist commented it as a common practice in their domain [29] [34]. The doctor, though having few experiences in viewing the p-value image, mentioned that he was aware of the statistical tests and would be prepared to learn to work with the p-value visualization.

7 Discussion

From the neuroscience perspective, we find that diffusion features on brain connectivity are quite effective in identifying AD patients from the controls. Meanwhile, geometric features of brain fibers, not as expected by domain experts, are often indistinguishable

between diseased and healthy brain networks. This result may imply that the destruction of white matter in AD patient's brains happens mostly at a microscopic scale, which does not heavily affect the morphology of brain fibers.

From the visualization perspective, we acknowledge that both SciVis/InfoVis and visual analytics (VA) techniques are necessary for the application of complex brain network visual comparison. InfoVis methods such as network creation, aggregation, and visualization help to generate overview pictures for comparison. VA methods combining feature selection algorithms help to identify significant differences/changes among the networks. Finally, SciVis methods help to drill down and review details of the network difference in the context of raw brain imaging data.

From the data analysis perspective, our system could be generalized to compare many other multivariate networks whose connections are defined by multiple features. For example, the academic networks with co-authorship and citation relationships are compared over time for evolution analysis of the community. The urban mobility network can be compared over the traffic volume or traffic speed feature between weekdays and weekends.

While the combination of statistical tests and visualization in one framework helps to solve the target visual analytics problem, we caution the risk of data dredging. Though the presented discriminative features are all significantly different between the comparing subject group, as too many of these features are reported, a few features could be false positives, i.e., not having true differences between the groups.

8 Conclusion

This paper describes MV^{2}Net, a visual analytics system designed to meet three key requirements of domain users: understand the role of multiple connectivity features in differentiating brain networks of contrasting subject groups, visually detect bio-markers from multiple feature comparisons, be aware of and resolve the data quality issue in neuroimaging and brain network construction process. In this system, we introduce several new techniques, which are demonstrated to be effective in bio-marker detection case studies between the brain networks of AD patients and healthy controls. First, the wrangling mechanism is shown to be useful as there are reasonable changes on the brain network after filtering out low-quality brain connections. Second, our result on brain network comparison reveals a less significant difference in the original connection strength feature than the diffusion features of FA/MD/RD/AxD. This validates the necessity for multiple feature comparisons. Notably, some established connectivity bio-markers of AD are found in our study by correlating the group-level difference on multiple diffusion features. Third, the multi-view visualization design illustrates the progressive change of brain networks during the development of AD. The additional fiber tract view helps to drill down to the voxel-level bio-markers.

In the future, we plan to apply the system to the analysis of functional brain networks. The problems defined in this work on structural brain networks are also important for functional brain networks. There are multiple fMRI modalities in measuring brain activity, e.g., blood-oxygen-level-dependent (BOLD) signal, EEG, and MEG. These signals can be correlated among ROIs using different algorithms and various lengths of sliding time windows. The resulting multiple functional connectivity features can be displayed and analyzed in our system. Meanwhile, the measurement of brain activity is often noisy, as discussed in the literature [81]. The interactive wrangling interface in our system could help to alleviate the data uncertain issue. Regularly, the functional brain networks are compared among multiple groups, e.g., in resting and several other cognitive task states. More importantly, it is critical to compare the functional networks in multiple time windows for temporal connectivity analysis.

Acknowledgments

This work was supported by NSFC Grants 61772504, U1609217, the Fundamental Research Funds for the Central Universities, and SKLSDE. Jun Tao and Yanjun Wu are corresponding authors.

References

[1] M. Daianu, N. Jahanshad, T. M. Nir, A. W. Toga, C. R. Jack Jr, M. W. Weiner, and P. M. Thompson, for the Alzheimer's Disease Neuroimaging Initiative, "Breakdown of brain connectivity between normal aging and alzheimer's disease: a structural k-core network analysis," *Brain connectivity*, vol. 3, no. 4, pp. 407–422, 2013.

[2] M. Kubicki, R. McCarley, C.-F. Westin, H.-J. Park, S. Maier, R. Kikinis, F. A. Jolesz, and M. E. Shenton, "A review of diffusion tensor imaging studies in schizophrenia," *Journal of psychiatric research*, vol. 41, no. 1-2, pp. 15–30, 2007.

[3] E. M. Kaye, "Update on genetic disorders affecting white matter," *Pediatric neurology*, vol. 24, no. 1, pp. 11–24, 2001.

[4] M. Gleicher, D. Albers, R. Walker, I. Jusufi, C. D. Hansen, and J. C. Roberts, "Visual comparison for information visualization," *Information Visualization*, vol. 10, no. 4, pp. 289–309, 2011.

[5] M. H. Everts, H. Bekker, J. B. Roerdink, and T. Isenberg, "Depth-dependent halos: Illustrative rendering of dense line data," *IEEE Transactions on Visualization and Computer Graphics*, vol. 15, no. 6, 2009.

[6] M. H. Everts, E. Begue, H. Bekker, J. B. Roerdink, and T. Isenberg, "Exploration of the brain's white matter structure through visual abstraction and multi-scale local fiber tract contraction," *IEEE Transactions on Visualization and Computer Graphics*, vol. 21, no. 7, pp. 808–821, 2015.

[7] M. Xia, J. Wang, and Y. He, "BrainNet Viewer: a network visualization tool for human brain connectomics," *PloS one*, vol. 8, no. 7, p. e68910, 2013.

[8] O. Sporns, *Networks of the Brain*. MIT press, 2011.

[9] E. Bullmore and O. Sporns, "Complex brain networks: graph theoretical analysis of structural and functional systems," *Nature Reviews Neuroscience*, vol. 10, no. 3, p. 186, 2009.

[10] K. J. Worsley, J.-I. Chen, J. Lerch, and A. C. Evans, "Comparing functional connectivity via thresholding correlations and singular value decomposition," *Philosophical Transactions of the Royal Society B: Biological Sciences*, vol. 360, no. 1457, pp. 913–920, 2005.

[11] R. Salvador, J. Suckling, M. R. Coleman, J. D. Pickard, D. Menon, and E. Bullmore, "Neurophysiological architecture of functional magnetic resonance images of human brain," *Cerebral Cortex*, vol. 15, no. 9, pp. 1332–1342, 2005.

[12] J. McGonigle, A. L. Malizia, and M. Mirmehdi, "Visualizing functional connectivity in fmri using hierarchical edge bundles," in *OHBM'11*, 2011.

[13] E. J. Sanz-Arigita, M. M. Schoonheim, J. S. Damoiseaux, S. A. Rombouts, E. Maris, F. Barkhof, P. Scheltens, and C. J. Stam, "Loss of 'small-world' networks in Alzheimer's disease: graph analysis of fMRI resting-state functional connectivity," *PloS one*, vol. 5, no. 11, 2010.

[14] M. Ghoniem, J.-D. Fekete, and P. Castagliola, "A comparison of the readability of graphs using node-link and matrix-based representations," in *InfoVis'04*, 2004, pp. 17–24.

[15] B. Alper, B. Bach, N. Henry Riche, T. Isenberg, and J.-D. Fekete, "Weighted graph comparison techniques for brain connectivity analysis," in *CHI'13*, 2013, pp. 483–492.

[16] X. Yang, L. Shi, M. Daianu, H. Tong, Q. Liu, and P. Thompson, "Blockwise human brain network visual comparison using nodetrix representation," *IEEE Transactions on Visualization and Computer Graphics*, vol. 23, no. 1, pp. 181–190, 2017.

[17] A. Pandey, H. Shukla, G. S. Young, L. Qin, A. A. Zamani, L. Hsu, R. Huang, C. Dunne, and M. A. Borkin, "CerebroVis: Designing an Abstract yet Spatially Contextualized Cerebral Artery Network Visualization," *IEEE Transactions on Visualization and Computer Graphics*, vol. 26, no. 1, pp. 938–948, 2019.

[18] B. Bach, E. Pietriga, and J.-D. Fekete, "Visualizing dynamic networks with matrix cubes," in *CHI'14*. ACM, 2014, pp. 877–886.

[19] B. Bach, N. Henry-Riche, T. Dwyer, T. Madhyastha, J.-D. Fekete, and T. Grabowski, "Small MultiPiles: Piling time to explore temporal patterns in dynamic networks," in *Computer Graphics Forum*, vol. 34, no. 3. Wiley Online Library, 2015, pp. 31–40.

[20] B. Bach, C. Shi, N. Heulot, T. Madhyastha, T. Grabowski, and P. Dragicevic, "Time curves: Folding time to visualize patterns of temporal evolution in data," *IEEE Transactions on Visualization and Computer Graphics*, vol. 22, no. 1, pp. 559–568, 2016.

[21] A. K. Al-Awami, J. Beyer, H. Strobelt, N. Kasthuri, J. W. Lichtman, H. Pfister, and M. Hadwiger, "NeuroLines: a subway map metaphor for visualizing nanoscale neuronal connectivity," *IEEE Transactions on Visualization and Computer Graphics*, vol. 20, no. 12, pp. 2369–2378, 2014.

[22] H. Mohammed, A. K. Al-Awami, J. Beyer, C. Cali, P. Magistretti, H. Pfister, and M. Hadwiger, "Abstractocyte: A visual tool for exploring nanoscale astroglial cells," *IEEE Transactions on Visualization and Computer Graphics*, vol. 24, no. 1, pp. 853–861, 2018.

[23] D. S. Margulies, J. Böttger, A. Watanabe, and K. J. Gorgolewski, "Visualizing the human connectome," *NeuroImage*, vol. 80, pp. 445–461, 2013.

[24] H. Pfister, V. Kaynig, C. P. Botha, S. Bruckner, V. J. Dercksen, H.-c. Hege, and J. B. T. M. Roerdink, "Visualization in connectomics," in *Scientific Visualization*. Springer, 2014, pp. 221–245.

[25] M. Wattenberg, "Visual exploration of multivariate graphs," in *CHI'06*, 2006, pp. 811–819.

[26] B. Shneiderman and A. Aris, "Network visualization by semantic substrates," *IEEE Transactions on Visualization and Computer Graphics*, vol. 12, no. 5, pp. 733–740, 2006.

[27] C. Nobre, M. Streit, and A. Lex, "Juniper: A tree+ table approach to multivariate graph visualization," *IEEE Transactions on Visualization & Computer Graphics*, no. 1, pp. 544–554, 2019.

[28] D. K. Jones, T. R. Knösche, and R. Turner, "White matter integrity, fiber count, and other fallacies: the do's and don'ts of diffusion MRI," *Neuroimage*, vol. 73, pp. 239–254, 2013.

[29] Y. Jin, C. Huang, M. Daianu, L. Zhan, E. L. Dennis, R. I. Reid, C. R. Jack Jr, H. Zhu, and P. M. Thompson, "3D tract-specific local and global analysis of white matter integrity in Alzheimer's disease," *Human brain mapping*, vol. 38, no. 3, pp. 1191–1207, 2017.

[30] C. Nobre, M. Meyer, M. Streit, and A. Lex, "The state of the art in visualizing multivariate networks," in *Computer Graphics Forum*, vol. 38, no. 3, 2019, pp. 807–832.

[31] D. Guo, "Flow mapping and multivariate visualization of large spatial interaction data," *IEEE Transactions on Visualization and Computer Graphics*, vol. 15, no. 6, pp. 1041–1048, 2009.

[32] B. H. Junker, C. Klukas, and F. Schreiber, "Vanted: a system for advanced data analysis and visualization in the context of biological networks," *BMC bioinformatics*, vol. 7, no. 1, p. 109, 2006.

[33] S. Schöffel, J. Schwank, and A. Ebert, "A user study on multivariate edge visualizations for graph-based visual analysis tasks," in *IV'16*, 2016, pp. 165–170.

[34] D. Jönsson, A. Bergström, C. Forsell, R. Simon, M. Engström, S. Walter, A. Ynnerman, and I. Hotz, "Visualneuro: A hypothesis formation and reasoning application for multi-variate brain cohort study data," *Computer Graphics Forum*, vol. 39, no. 6, pp. 392–407, 2020.

[35] M. Gleicher, "Considerations for visualizing comparison," *IEEE Transactions on Visualization and Computer Graphics*, vol. 24, no. 1, pp. 413–423, 2017.

[36] A. Dasgupta, J. Poco, Y. Wei, R. Cook, E. Bertini, and C. T. Silva, "Bridging theory with practice: An exploratory study of visualization use and design for climate model comparison," *IEEE Transactions on Visualization and Computer Graphics*, vol. 21, no. 9, pp. 996–1014, 2015.

[37] J. Schmidt, M. E. Gröller, and S. Bruckner, "Vaico: Visual analysis for image comparison," *IEEE Transactions on Visualization and Computer Graphics*, vol. 19, no. 12, pp. 2090–2099, 2013.

[38] E. S. Finn, X. Shen, D. Scheinost, M. D. Rosenberg, J. Huang, M. M. Chun, X. Papademetris, and R. T. Constable, "Functional connectome fingerprinting: identifying individuals using patterns of brain connectivity," *Nature neuroscience*, vol. 18, no. 11, p. 1664, 2015.

[39] R. D. Airan, J. T. Vogelstein, J. J. Pillai, B. Caffo, J. J. Pekar, and H. I. Sair, "Factors affecting characterization and localization of interindividual differences in functional connectivity using mri," *Human brain mapping*, vol. 37, no. 5, pp. 1986–1997, 2016.

[40] T. Fujiwara, J.-K. Chou, A. M. McCullough, C. Ranganath, and K.-L. Ma, "A visual analytics system for brain functional connectivity comparison across individuals, groups, and time points," in *PacificVis'17*, 2017, pp. 250–259.

[41] L. Shi, H. Tong, and X. Mu, "BrainQuest: Perception-guided brain network comparison," in *ICDM'15*, 2015, pp. 379–388.

[42] L. Shi, H. Tong, M. Daianu, F. Tian, and P. M. Thompson, "Visual analysis of brain networks using sparse regression models," *ACM Transactions on Knowledge Discovery from Data*, vol. 12, no. 1, pp. 1–30, 2018.

[43] C. Readhead, D. H. Laidlaw, E. T. Ahrens, M. J. Avalos, and R. E. Jacobs, "Visualizing diffusion tensor images of the mouse spinal cord," in *VIS'98*, 1998, pp. 127–134.

[44] S. Zhang, Ç. Demiralp, and D. H. Laidlaw, "Visualizing diffusion tensor MR images using streamtubes and streamsurfaces," *IEEE Transactions on Visualization and Computer Graphics*, vol. 9, no. 4, pp. 454–462, 2003.

[45] P. Svetachov, M. H. Everts, and T. Isenberg, "DTI in context : Illustrating brain fiber tracts in situ," *Computer Graphics Forum*, vol. 29, no. 3, pp. 1023–1032, 2010.

[46] R. Brecheisen, B. Platel, B. M. ter Haar Romeny, and A. Vilanova, "Illustrative uncertainty visualization of DTI fiber pathways," *The Visual Computer*, vol. 29, no. 4, pp. 297–309, 2013.

[47] Z. Ding, J. C. Gore, and A. W. Anderson, "Classification and quantification of neuronal fiber pathways using diffusion tensor MRI," *Magnetic Resonance in Medicine*, vol. 49, no. 4, pp. 716–721, 2003.

[48] I. Corouge, S. Gouttard, and G. Gerig, "Towards a shape model of white matter fiber bundles using diffusion tensor MRI," in *ISBI'04*, 2004, pp. 344–347.

[49] A. Brun, H. Knutsson, H.-J. Park, M. E. Shenton, and C.-F. Westin, "Clustering fiber traces using normalized cuts," in *MICCAI'04*, 2004, pp. 1342–1353.

[50] B. Moberts, A. Vilanova, and J. J. van Wijk, "Evaluation of fiber clustering methods for diffusion tensor imaging," in *VIS'05*, 2005, pp. 65–72.

[51] R. Jianu, Ç. Demiralp, and D. H. Laidlaw, "Exploring 3D DTI fiber tracts with linked 2D representations," *IEEE Transactions on Visualization and Computer Graphics*, vol. 15, no. 6, pp. 1449–1456, 2009.

[52] A. C. Jalba, M. A. Westenberg, and J. B. T. M. Roerdink, "Interactive segmentation and visualization of DTI data using a hierarchical watershed representation," *IEEE Transactions on Image Processing*, vol. 24, no. 3, pp. 1025–1035, 2015.

[53] R. Brecheisen, B. Platel, A. Vilanova, and H. Romeny, "Parameter sensitivity visualization in DTI fiber tracking," *IEEE Transactions on Visualization and Computer Graphics*, vol. 15, no. 6, pp. 1441–1448, 2009.

[54] G. Wang, H. Chen, G. Chen, and W. Chen, "Visualizing differences of DTI fiber models using 2D normalized embeddings," in *PacificVis'14*, 2014, pp. 350–351.

[55] J. Chen, G. Zhang, W. Chiou, D. H. Laidlaw, and A. P. Auchus, "Measuring the effects of scalar and spherical colormaps on ensembles of dmri tubes," *IEEE Transactions on Visualization and Computer Graphics*, 2019.

[56] C. Hurter, N. H. Riche, S. M. Drucker, M. Cordeil, R. Alligier, and R. Vuillemot, "Fiberclay: Sculpting three dimensional trajectories to reveal structural insights," *IEEE Transactions on Visualization and Computer Graphics*, vol. 25, no. 1, pp. 704–714, 2018.

[57] P. J. Basser, J. Mattiello, and D. LeBihan, "MR diffusion tensor spectroscopy and imaging," *Biophysical journal*, vol. 66, no. 1, pp. 259–267, 1994.

[58] R. L. Buckner, A. Z. Snyder, B. J. Shannon, G. LaRossa *et al.*, "Molecular, structural, and functional characterization of alzheimer's disease: evidence for a relationship between default activity, amyloid, and memory," *Journal of Neuroscience*, vol. 25, no. 34, pp. 7709–7717, 2005.

[59] P. M. Thompson, M. S. Mega, R. P. Woods *et al.*, "Cortical change in alzheimer's disease detected with a disease-specific population-based brain atlas," *Cerebral Cortex*, vol. 11, no. 1, pp. 1–16, 2001.

[60] J. Han, M. Kamber, and J. Pei, *Data mining: concepts and techniques, third edition*. Morgan Kaufmann Publishers, 2012.

[61] "Alzheimer's Disease Neuroimaging Initiative. http://adni.loni.usc.edu/."

[62] "FreeSurfer. http://surfer.nmr.mgh.harvard.edu/," 2012.

[63] R. S. Desikan, F. Ségonne, B. Fischl *et al.*, "An automated labeling system for subdividing the human cerebral cortex on mri scans into gyral based regions of interest," *Neuroimage*, vol. 31, no. 3, pp. 968–980, 2006.

[64] T. M. Nir, N. Jahanshad, J. E. Villalon-Reina, A. W. Toga, C. R. Jack, M. W. Weiner, and P. M. Thompson, "Effectiveness of regional DTI measures in distinguishing Alzheimer's disease, MCI, and normal aging," *NeuroImage: clinical*, vol. 3, pp. 180–195, 2013.

[65] D. Jones, "Tractography Gone Wild: Probabilistic Fibre Tracking Using the Wild Bootstrap With Diffusion Tensor MRI," *IEEE Transactions on Medical Imaging*, vol. 27, no. 9, pp. 1268–1274, 2008.

[66] "Lobes of the brain. https://en.wikipedia.org/wiki/lobes_of_the_brain."

[67] D. Merhof, M. Sonntag, F. Enders, C. Nimsky, P. Hastreiter, and G. Greiner, "Hybrid visualization for white matter tracts using trian-

gle strips and point sprites," *IEEE Transactions on Visualization and Computer Graphics*, vol. 12, no. 5, pp. 1181–1188, 2006.
[68] J. W. Wallis, T. R. Miller, C. A. Lerner, and E. C. Kleerup, "Three-dimensional display in nuclear medicine," *IEEE Transactions on Medical Imaging*, vol. 8, no. 4, pp. 297–303, 1989.
[69] C. Beaulieu, "The basis of anisotropic water diffusion in the nervous system–a technical review," *NMR in Biomedicine*, vol. 15, no. 7-8, pp. 435–455, 2002.
[70] S.-K. Song, J. Yoshino, T. Q. Le, S.-J. Lin, S.-W. Sun, A. H. Cross, and R. C. Armstrong, "Demyelination increases radial diffusivity in corpus callosum of mouse brain," *Neuroimage*, vol. 26, no. 1, pp. 132–140, 2005.
[71] R. Della Nave, A. Ginestroni, S. Diciotti, E. Salvatore, A. Soricelli, and M. Mascalchi, "Axial diffusivity is increased in the degenerating superior cerebellar peduncles of friedreich's ataxia," *Neuroradiology*, vol. 53, no. 5, pp. 367–372, 2011.
[72] A. W. Toga and P. M. Thompson, "Mapping brain asymmetry," *Nature Reviews Neuroscience*, vol. 4, no. 1, pp. 37–48, 2003.
[73] S. J. Teipel, W. Bayer, G. E. Alexander, Y. Zebuhr, D. Teichberg, L. Kulic, M. B. Schapiro, H.-J. Möller, S. I. Rapoport, and H. Hampel, "Progression of corpus callosum atrophy in alzheimer disease," *Archives of Neurology*, vol. 59, no. 2, pp. 243–248, 2002.
[74] P. R. Hof, J. H. Morrison, and K. Cox, "Quantitative analysis of a vulnerable subset of pyramidal neurons in alzheimer's disease: I. superior frontal and inferior temporal cortex," *Journal of Comparative Neurology*, vol. 301, no. 1, pp. 44–54, 1990.
[75] L.-F. Lue, L. Brachova, W. H. Civin, and J. Rogers, "Inflammation, aβ deposition, and neurofibrillary tangle formation as correlates of alzheimer's disease neurodegeneration," *Journal of neuropathology & experimental neurology*, vol. 55, no. 10, pp. 1083–1088, 1996.
[76] S. W. Scheff, D. A. Price, F. A. Schmitt, M. A. Scheff, and E. J. Mufson, "Synaptic loss in the inferior temporal gyrus in mild cognitive impairment and alzheimer's disease," *Journal of Alzheimer's Disease*, vol. 24, no. 3, pp. 547–557, 2011.
[77] N. Hirono, E. Mori, K. Ishii *et al.*, "Frontal lobe hypometabolism and depression in alzheimer's disease," *Neurology*, vol. 50, no. 2, pp. 380–383, 1998.
[78] A. M. Palmer and M. A. Burns, "Selective increase in lipid peroxidation in the inferior temporal cortex in alzheimer's disease," *Brain research*, vol. 645, no. 1-2, pp. 338–342, 1994.
[79] P. S. Aisen, R. C. Petersen, M. C. Donohue, A. Gamst *et al.*, "Clinical core of the alzheimer's disease neuroimaging initiative: progress and plans," *Alzheimer's & Dementia*, vol. 6, no. 3, pp. 239–246, 2010.
[80] P. T. Nelson, E. Head, F. A. Schmitt *et al.*, "Alzheimer's disease is not "brain aging": neuropathological, genetic, and epidemiological human studies," *Acta neuropathologica*, vol. 121, no. 5, pp. 571–587, 2011.
[81] M. de Ridder, K. Klein, and J. Kim, "A review and outlook on visual analytics for uncertainties in functional magnetic resonance imaging," *Brain informatics*, vol. 5, no. 2, p. 5, 2018.

Lei Shi is a professor in ACT/BDBC/SKLSDE, School of Computer Science and Engineering, Beihang University. Previously, he was a professor in SKLCS, Institute of Software, Chinese Academy of Sciences and a research manager in IBM research - China. He holds B.S./M.S./Ph.D. degrees from Department of Computer Science and Technology, Tsinghua University. His research interests span Visualization, Visual Analytics, and Data Mining. He is the recipient of VAST Challenge Award in 2010 and 2012.

Junnan Hu is a graduate student in Computer Science at Sun Yat-sen University. Her research interests involved in Scientific Visualization and Visual Analytics.

Zhihao Tan is a graduate student in Institute of Software, Chinese Academy of Sciences. He received his B.S. degree from Beijing Jiaotong University. His research interests include Visual Analytics and Data Mining.

Jun Tao is an associate professor at School of Data and Computer Science in Sun Yat-sen University and National Supercomputer Center at Guangzhou. Previously, he was a postdoctral researcher at University of Notre Dame. He received bachelor degree from Sun Yat-sen University in 2008 and Ph.D. degree from Michigan Technological University in 2015. His research interests include scientific visualization and visual analytics, with an emphasize on flow visualization and exploratory tools for scientific datasets.

Jiayan Ding is a first-year graduate student majoring in interactive design in college of design and innovation, Tongji University.

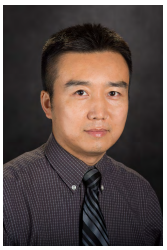

Yan Jin is a research scientist at the Department of Radiation Oncology in the University of Texas MD Anderson Cancer Center. He received his Ph.D. degree in Biomedical Engineering from the University of California, Los Angeles in 2014. He specializes in Medical Imaging, especially in various neurological diseases, such as Alzheimer's disease. He has over 50 publications and is well recognized internationally with thousands of citations for his work.

Yanjun Wu received the Ph.D. degree in computer science from the Institute of Software, Chinese Academy of Sciences (ISCAS), Beijing, China. He is currently a Research Professor with ISCAS. His research interests include operating systems and system security.

Paul M. Thompson received the bachelor's degree in Greek and Latin languages and mathematics and the master's degree in mathematics from Oxford University in 1991 and 1993, respectively, and the Ph.D. degree in neuroscience from the University of California at Los Angeles in 1998. He is currently a Professor of neurology with the Imaging Genetics Center (IGC), University of Southern California, Los Angeles. He specializes in the field of human-brain imaging, with a research interest in mathematical and computational algorithm development for human-brain mapping. He has contributed to more than 900 publications. He currently leads the Enhancing Neuro Imaging Genetics through Meta Analysis (ENIGMA) project, a global data collection and sharing effort designed to understand how brain structure changes during the trajectory of brain atrophy, mental illness and Alzheimer's, and the underlying genetic landscape.